Impact of [110]/(001) uniaxial stress on valence band structure and hole effective mass of silicon*

Ma Jianli(马建立)†, Zhang Heming(张鹤鸣), Song Jianjun(宋建军), Wang Guanyu(王冠宇), Wang Xiaoyan(王晓艳), and Xu Xiaobo(徐小波)

Key Laboratory of Ministry of Education for Wide Band-Gap Semiconductor Materials and Devices, Xidian University, Xi'an 710071, China

Abstract: The valence band structure and hole effective mass of silicon under a uniaxial stress in (001) surface along the [110] direction were detailedly investigated in the framework of the $\boldsymbol{k\cdot p}$ theory. The results demonstrated that the splitting energy between the top band and the second band for uniaxial compressive stress is bigger than that of the tensile one at the same stress magnitude, and of all common used crystallographic direction, such as [110], [001], [$\bar{1}$10] and [100], the effective mass for the top band along [110] crystallographic direction is lower under uniaxial compressive stress compared with other stresses and crystallographic directions configurations. In view of suppressing the scattering and reducing the effective mass, the [110] crystallographic direction is most favorable to be used as transport direction of the charge carrier to enhancement mobility when a uniaxial compressive stress along [110] direction is applied. The obtained results can provide a theory reference for the design and the selective of optimum stress and crystallorgraphic direction configuration of uniaxial strained silicon devices.

Key words: valence band structure; uniaxial strained silicon; $\boldsymbol{k\cdot p}$ method

DOI: 10.1088/1674-4926/32/2/022002 **PACC:** 7366F; 7125C; 7115M

1. Introduction

The use of stress-induced mobility enhancement to achieve better p-type metal–oxide–semiconductor field-effect transistors (p-MOSFETs) performance has spurred great research interest in recent years[1, 2]. The way to introduce stress to the channel, including the substrate-induced biaxial stress and process-induced uniaxial stress[3]. Currently, most studies mainly concentrate on the effect of biaxial stress on the electric-characteristics of silicon material, inversion layer, and MOSFET[1, 4, 5]. Recently, the effect of biaxial stress on the valence band structure of silicon material has been intensively investigated[6−8]. However, few studies focus on the impact of uniaxial stress on the valence band structure of silicon material.

It has been demonstrated that the large hole mobility gain can be obtained under uniaxial stress along the ⟨110⟩ directions in p-MOSFETs[9, 10]. Stress in the ⟨110⟩ direction can induce significant shear lattice distortion, however, the influence of uniaxial stress-induced shear distortion on the valence band structure and effective mass has not yet been carefully analyzed due to the complicated valence band structure of silicon, and the usual qualitative described of valence band structure are not suitable for device simulation and design[6, 11]. Therefore, a comprehensive and quantitative described of the valence band structure of uniaxial strained silicon is needed.

In this paper, to obtain the E–k relation of valence band of uniaxial strained silicon, the $\boldsymbol{k\cdot p}$ method is utilized due to its simplicity and accuracy in modeling the valence band properties in the vicinity of the Γ point. The uniaxial stress in the [110] direction of ⟨001⟩ surface is considered since it is common used in p-MOSFETs technology. By using the obtained E–k relation, the energy level shift and the splitting energy between the top valence band and the second valence band with stress at the Γ point was extracted, and the valence band warped with stress, which can be described by effective mass was quantitative evaluated.

2. Calculated models

2.1. Valence band structure model

The valence band structure of unstrained silicon can be obtained by calculating the eigenvalues of $H_{\boldsymbol{k\cdot p}}$. The effect of the spin-orbit interaction and strain on the valence band structure is included by adding perturbation matrices $H_{\mathrm{S.O.}}$ and H_{strain} to $H_{\boldsymbol{k\cdot p}}$. Thus, the total Hamiltonian H for uniaxial strained silicon consists of three parts:

$$H = H_{\boldsymbol{k\cdot p}} + H_{\mathrm{S.O.}} + H_{\mathrm{strain}}, \tag{1}$$

where the $H_{\mathrm{S.O.}}$ and H_{strain} represent the spin-orbit interaction and strain Hamiltonian, respectively. The $H_{\boldsymbol{k\cdot p}}$, $H_{\mathrm{S.O.}}$, and H_{strain} are all 6×6 matrices, and the expressions of the three terms are given in Ref. [12]. By diagonalizing the matrix of H yields three distinct eigenvalues as[13]

* Project supported by the National Ministries and Commissions of China (Nos. 51308040203, 6139801), the Fundamental Research Funds for the Central Universities of China (No. 72105499), and the Natural Science Basic Research Plan in Shaanxi Province of China (No. 2010JQ8008).

† Corresponding author. Email: jianlima2005@126.com

Received 11 July 2010, revised manuscript received 24 August 2010

Table 1. Parameters for the valence band model calculation of silicon.

S_{11}, S_{12}, S_{44} (cm^2/dyn)	L, M, N	l, m, n (eV)	Δ (eV)
7.69×10^{-13}, -2.44×10^{-13}, 1.25×10^{-12}	–5.78, –3.44, –8.64	–0.15, 6.84, –5.89	0.044

$$\begin{cases} E_{\rm v}^1 = 2\sqrt{Q}\cos\dfrac{\Theta}{3} - \dfrac{p}{3}, \\ E_{\rm v}^2 = 2\sqrt{Q}\cos\dfrac{\Theta+2\pi}{3} - \dfrac{p}{3}, \\ E_{\rm v}^3 = 2\sqrt{Q}\cos\dfrac{\Theta-2\pi}{3} - \dfrac{p}{3}. \end{cases} \tag{2}$$

where the $E_{\rm v}^1$, $E_{\rm v}^2$, and $E_{\rm v}^3$ are the energies for the top valence band, the second valence band (usually called as the "heavy hole" band and "light hole" band) and spin-orbit coupling band, respectively. The "top" and "second" bands indicate the splitting energy levels in a descending energy order. Here

$$\begin{cases} Q = (p^2 - 3q)/9, \\ R = (2p^3 - 9pq + 27r)/54, \\ \Theta = \arccos(-R/\sqrt{Q^3}), \end{cases} \tag{3}$$

and

$$\begin{aligned} p &= \Delta - (a_{11} + a_{22} + a_{33}), \\ q &= a_{11}a_{22} + a_{22}a_{33} + a_{33}a_{11} - a_{12}^2 - a_{13}^2 - a_{23}^2 \\ &\quad - (2\Delta/3)(a_{11} + a_{22} + a_{33}), \\ r &= a_{11}a_{23}^2 + a_{22}a_{13}^2 + a_{33}a_{12}^2 - a_{11}a_{22}a_{33} \\ &\quad - 2a_{12}a_{23}a_{13} + (\Delta/3)(a_{11}a_{22} + a_{22}a_{33} + a_{33}a_{11} \\ &\quad - a_{12}^2 - a_{13}^2 - a_{23}^2). \end{aligned} \tag{4}$$

The $a_{\alpha\beta}$ is the element of matrix $H_{\boldsymbol{k}\cdot\boldsymbol{p}} + H_{\rm strain}$, which can be expressed as

$$a_{\alpha\beta} = \begin{cases} Lk_\alpha^2 + M(k_\beta^2 + k_\gamma^2) + l\varepsilon_{\alpha\alpha} + m(\varepsilon_{\beta\beta} + \varepsilon_{\gamma\gamma}), & \alpha = \beta, \\ Nk_\alpha k_\beta + n\varepsilon_{\alpha\beta}, & \alpha \neq \beta, \end{cases} \tag{5}$$

the induces α, β, γ equal (x, y, z) or $(1, 2, 3)$. The parameters L, M, N are the dimensionless terms, which are related to the effect of the conduction band on the valence band. The l, m, n are three independent valence band deformation potential parameters. The Δ denotes the Brillouin zone center ($k = 0$) spin-orbit splitting energy. The ε represents the strain tensor, and the strain tensors for uniaxial stress in the [110] direction of (001) surface are

$$\varepsilon = \begin{bmatrix} \dfrac{1}{2}T(s_{11} + s_{12}) & \dfrac{1}{4}Ts_{44} & 0 \\ \dfrac{1}{4}Ts_{44} & \dfrac{1}{2}T(s_{11} + s_{12}) & 0 \\ 0 & 0 & Ts_{12} \end{bmatrix}, \tag{6}$$

where s_{11}, s_{12}, s_{44} are cubic compliance constants of silicon material, and T the magnitude of uniaxial stress in units of GPa (The positive stress corresponds to the tensile stress, and the negative stress to compressive stress in subsequent discussion.). As ε is a function of T, so $E_{\rm v}^1$, $E_{\rm v}^2$, $E_{\rm v}^3$ are also functions of T. The parameters employed in the calculations are listed in Table 1.

Let $(k_\alpha, k_\beta, k_\gamma)$ along one crystallographic direction, we will get E–k relation of the crystallographic direction under uniaxial stress, and let $(k_\alpha, k_\beta, k_\gamma) = 0$, we will get the energy of the Γ point (the center of Brillouin zone) as a function of stress.

2.2. Effective mass model

The external uniaxial stress induces a change in the curvature of valence band in the vicinity of the Γ point, and the valence band edge warped under uniaxial stress can be evaluated by effective mass. The effective mass is calculated from the E–k relation by[14]

$$\frac{1}{m_{\rm i}^*} = \frac{1}{h^2}\left(\frac{{\rm d}^2E}{{\rm d}k_{\rm i}^2}\right)_{k=0}. \tag{7}$$

Here, the index i indicates the crystal direction of interest, E is the energy of valence band, h is Plack constant, and k denotes the wave vector. According to Eq. (7), we can obtain the effective mass along one crystallographic direction at the Γ point under uniaxial stress.

3. Results and discussion

3.1. Shift and split of the valence band energy level

The valence band energy as a function of wave vectors k along the [110], [001], [$\bar{1}$10] and [100] crystallographic directions near the Γ point under different stresses is shown in Figs. 1(a) and 1(b). It is shown that the topmost valence bands are degenerated at the Γ point at unstressed condition. When uniaxial stress is applied, stress induced the band shift, and removed the degeneracy of the topmost valence band at the Γ point, which can be explained from the fact that: crystal symmetry determines the symmetry of the band structure, when a uniaxial stress along the [110] direction applied to the silicon crystal, which breaks the crystal symmetry, makes the crystal structure of silicon transform from the cubic system to orthorhombic system, thus the crystal symmetry is lowered, and causes the bands shift and splitting. Noted that the curvature of the bands was also altered under uniaxial stress, and the band curve along [110] crystallographic direction under 1 GPa uniaxial compressive stress was more warped than others. These band relative shifts, together with splitting of the topmost valence band, can cause a redistribution of carriers within the valence band and the suppression of the inter-band scattering, which can be expected to contribute to the hole mobility enhancement[6].

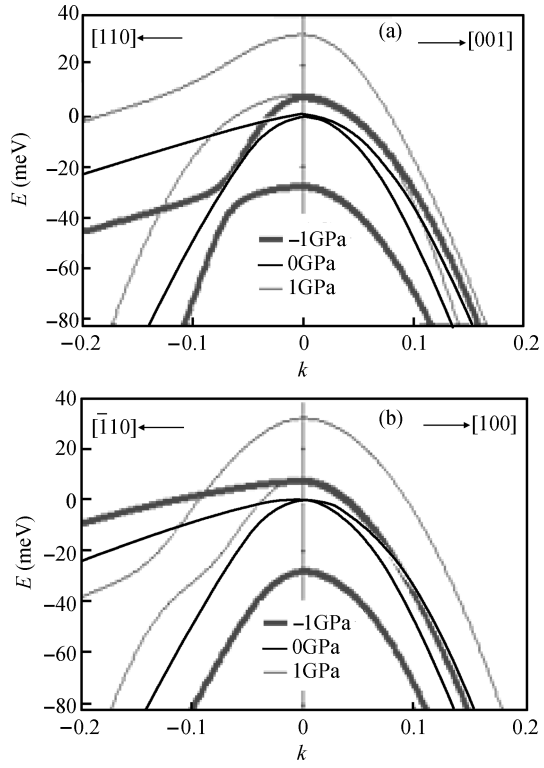

Fig. 1. Top and second valence bands energy versus wave vectors k near the Γ point under different uniaxial stresses. (a) E–k relation in [110] and [001] directions. (b) E–k relation in [$\bar{1}$10] and [100] directions.

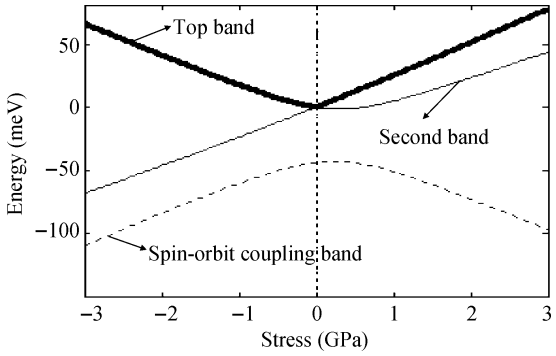

Fig. 2. Energy change in valence band edge as a function of applied uniaxial [110] direction stress.

From the above obtained valence band E–k relation, we can calculate the stress induced energy level shift and split at the Γ point. The energy level shift of the three topmost valence bands at the Γ point versus stress are shown in Fig. 2. It is shown that the top band energy level shift up whatever the sign of applied uniaxial stress, whereas the second band energy level shift down under uniaxial compressive stress, and shift up under uniaxial tensile stress. The splitting energy between the top band and the second band increase with the stress, and the splitting energy for uniaxial compressive stress is bigger than that of the tensile one at the same stress magnitude (see Fig. 3), which is advantageous to suppress the interband scattering. Hence, the uniaxial compressive stress is more significant than uniaxial tensile stress in terms of reduced scattering and enhanced carrier mobility.

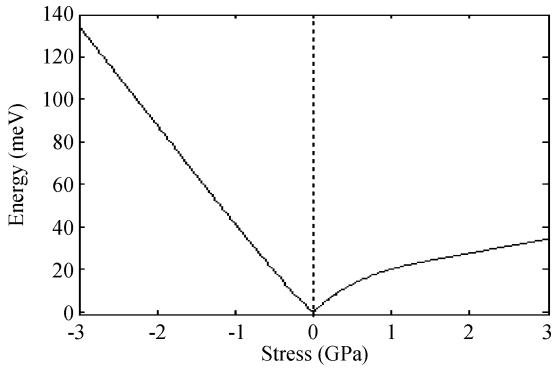

Fig. 3. Splitting energy of the subband as a function of applied uniaxial [110] direction stress.

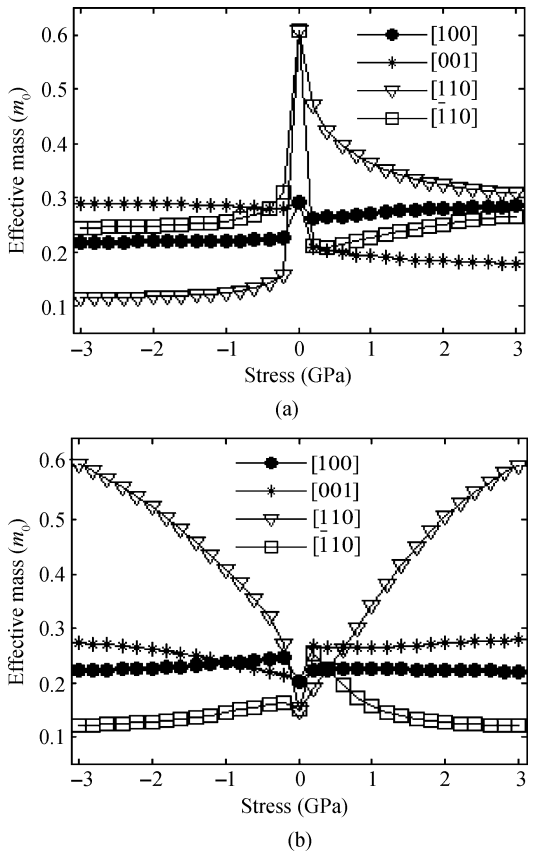

Fig. 4. Effective mass of different crystallographic directions as a function of applied uniaxial [110] direction stress. (a) Effective mass for the top band. (b) Effective mass for the second band.

3.2. Effective mass change due to [110] stress

The holes effective mass for the top and second valence bands along [100], [001], [110] and [$\bar{1}$10] crystallographic directions as a function of stress were numerically calculated and shown in Fig. 4, where the m_0 is the free electric mass. A dramatically anisotropy behavior of holes effective mass can be observed. The effective mass for the top band along [100] and [001] crystallographic directions, both first drop a little in the low stress region (less than 0.4 GPa), then are insensitive

Table 2. Calculated and experiment hole effective masses (unit: m_0) of unstressed silicon.

Method & Refs.	The top valence band masses		The second valence band masses	
	$m^{(100)}$	$m^{(110)}$	$m^{(100)}$	$m^{(110)}$
This work	0.29	0.60	0.20	0.15
EPM[2]	0.31	0.59	0.23	0.17
First principle[15]	0.22	0.36	0.22	0.17
First principle[16]	0.26	0.54	0.18	0.14
Experiment[17]	0.43	0.43	0.19	0.24
Experiment[16]	0.46	0.53	0.17	0.16

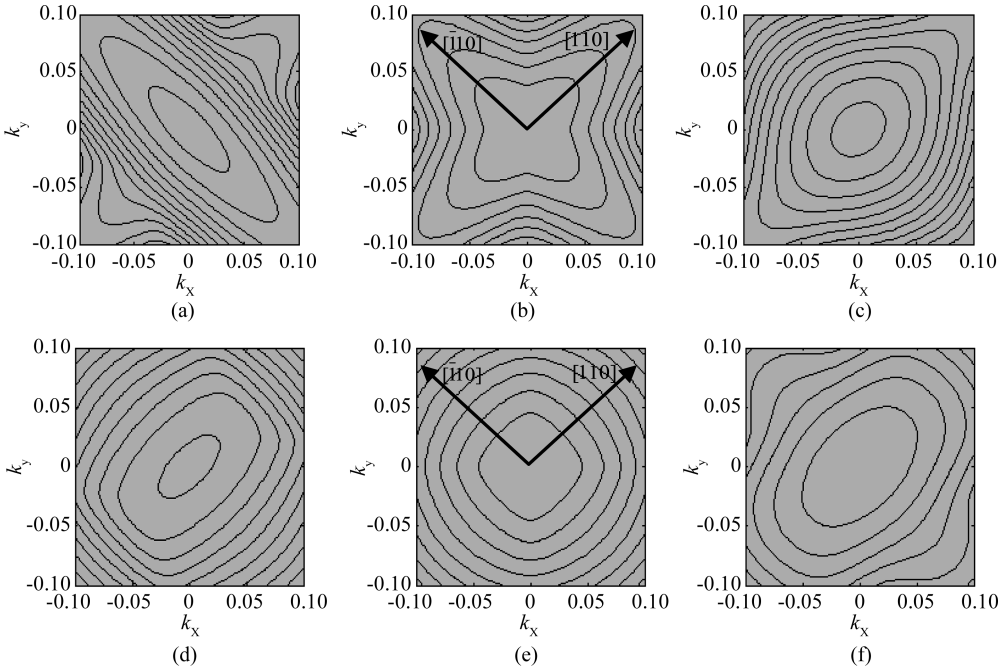

Fig. 5. 2D equi-energy surfaces for the top and second valence bands in silicon under uniaxial [110] direction stress. (a) 1 GPa compressive stress, (b) unstressed, and (c) 1 GPa tensile stress for the top band. (d) 1 GPa compressive stress, (e) unstressed, and (f) 1 GPa tensile stress for the second band. The energy interval between contours is 50 meV.

to the stress, whereas the effective mass for the second band along the two directions, both initially increase a little in the low stress region then nearly keep unchanged with stress. The effective mass along [110] crystallographic direction, for the top band effective mass, which drop dramatically from its initial value of $0.6m_0$ at zero stress to about $0.14m_0$ at about –0.4 GPa, then start to decrease slowly with further increasing in compressive stress, whereas it decrease gradually with stress when the uniaxial tensile stress is applied; for the second band effective mass, which shows a continuous increase trend with stress whatever the stress is compressive stress or tensile stress. The effective mass for the top band along [$\bar{1}$10] crystallographic direction, it also undergoes a sharp drop with the initial application stress and then decreases slowly with compressive stress, and increases with tensile stress. For the second band mass along [$\bar{1}$10] crystallographic direction, it first increases slightly with stress and then decreases slowly with further increase in stress whatever the sign of applied stress. Among these crystallographic directions, the effective mass for the top band along the [110] crystallographic direction is lower under uniaxial compressive stress than other stresses and crystallographic direction configurations. In general, the characteristic of hole transport is mainly governed by the properties of the top valence band since most of the holes are inclined to occupy the band with a lower energy. It suggested that [110] crystallographic direction can be used as transport direction of the charge carrier (conducting channel direction) to enhance mobility compared with other crystallographic directions.

Since the effective mass for the top and second band of silicon under uniaxial stress is lacking in theory and experiment, in order to validate the obtained calculation results, we compared our effective mass results with the available previous calculations and experiments of unstressed silicon in Table 2. For the top band masses, our results show a good agreement with empirical pseudopotential method calculation[2], but little bigger than the first principle results[6, 15], and compared with the experiment results[16, 17], the effective mass along [100] crystallographic direction are underestimated and the [110] crystallographic direction are overestimated by our calculations. The reason may be due to there being some deviations in fitting the curve to compute the second order differential, which needs to be further improved. Noted that our calculation results were consistent with other calculated and experiment results for the second valence band masses.

3.3. 2D equi-energy surface change due to [110] stress

To further illustrate the effective mass change under the uniaxial stress, the 2D equi-energy surfaces in the k_x–k_y plane for the top and second valence bands were shown in Fig. 5. It can be seen that for the unstressed silicon, the regions of the 2D equi-energy contours near the Γ point (see the inner rings) are close to a "star" shape for the top band, and a "rhombus" shape for the second band. When the 1 GPa uniaxial stress is applied, these regions are close to ellipsoidal shapes, and for the top band, the minor axis of the ellipse is along [110] crystallographic direction for the uniaxial compressive stress and $[\bar{1}10]$ direction for the tensile stress, while for the second band, the minor axis of the ellipse is along [110] crystallographic direction whatever the stress sign is. It is also shown that the energy contour of compressive stress is more warped than the tensile ones in the same stress magnitude. Energy contour warping can lead to the effective mass change. All of these imply that under uniaxial compressive stress, the change of hole effective mass along [110] crystallographic direction for the top band and $[\bar{1}10]$ direction for the second band is large compared with other stress and crystallographic direction configurations, which is consistent with our results of effective mass calculation. It is expected that the large change in effective mass can lead to larger mass-induced mobility change.

4. Conclusion

A detailed quantitative analysis of valence band structure and effective mass of silicon under a uniaxial stress in (001) surface along the [110] direction has been presented by employing six-band $\boldsymbol{k} \cdot \boldsymbol{p}$ perturbation theory. Stressed induced the valence band E–k relation change, valence band edge energy level shift, split, and the valence band warping which can be described by effective mass has been quantitatively evaluated. In view of suppressing the scattering and reducing the effective mass, when a uniaxial compressive stress in (001) surface along [110] direction is applied，the [110] crystallographic direction is most favorable to be used as transport direction of the charge carriers to enhancement hole mobility compared with other crystallographic directions. The obtained results provide a theory reference for the design and the selective of the optimum stress direction and transport direction of the charge carriers of uniaxial strained silicon devices.

References

[1] Sun G, Sun Y, Nishida T, et al. Hole mobility in silicon inversion layers: stress and surface orientation. J Appl Phys, 2007, 102(8): 084501
[2] Wang E X, Matagne P, Shifren L, et al. Physics of hole transport in strained silicon MOSFET inversion layers. IEEE Trans Electron Devices, 2006, 53(8): 1840
[3] Chee W, Maikop S, Yu C Y. Mobility enhancement technologies. IEEE Circuits Devices Mag, 2005, 21(3): 21
[4] Dhar S, Kosina H, Palankovski V, et al. Electronic mobility model for strained-Si devices. IEEE Trans Electron Devices, 2005, 52(4): 527
[5] Yang X, Lim J, Sun G, et al. Strain-induced changes in the gate tunneling currents in p-channel metal–oxide–semiconductor field-effect transistors. Appl Phys Lett, 2006, 88(5): 052108
[6] Yu D, Zhang Y, Liu F. First-principles study of electronic properties of biaxially strained silicon: effects on charge carrier mobility. Phys Rev B, 2008, 78(24): 245204
[7] Song J J, Zhang H M, Hu H Y, et al. Calculation of band structure in (101)-biaxially strained Si. Sci China Ser G: Phys Mech Astron, 2009, 52(4): 546
[8] Kima J, Fischetti M V. Electronic band structure calculations for biaxially strained Si, Ge, and III–V semiconductors. J Appl Phys, 2010, 108(1): 013710
[9] Giles M D, Armstrong M, Auth C, et al. Understanding stress enhanced performance in Intel 90 nm CMOS technology. VLSI Symp Tech Dig, 2004, 12(2): 118
[10] Shifren L, Wang X, Matagne P, et al. Drive current enhancement in p-type metal–oxide–semiconductor field-effect transistors under shear uniaxial stress. Appl Phys Lett, 2004, 85(25): 6188
[11] Sun G, Parthasarathy S, Thompson S E. Physics of process induced uniaxially strained Si. Mater Sci Eng B, 2006, 135(3): 179
[12] Hinckley J M, Singh J. Influence of substrate composition and crystallographic orientation on the band structure of pseudomorphic Si–Ge alloy films. Phys Rev B, 1990, 42(6): 3546
[13] Dijkstra J E, Wenckebach W T. Hole transport in strained Si. J Appl Phys, 1997, 81(3): 1259
[14] Xie X D, Lu D. Energy band theory of solids. Shanghai: Fudan University Press, 1998
[15] Ramos L E, Teles L K, Scolfaro L M R, et al. Structural, electronic, and effective-mass properties of silicon and zinc-blende group-III nitride semiconductor compounds. Phys Rev B, 2001, 63(16): 165210
[16] Dexter R N, Zeiger H J, Lax B. Cyclotron resonance experiments in silicon and germanium. Phys Rev, 1956, 104(3): 637
[17] Dexter R N, Lax B. Effective masses of holes in silicon. Phys Rev, 1954, 96(1): 223